

Cascading-driven Intentional Controlled Islanding for Enhancing Power Grid Operational Resilience

Sina Hashemi, *Member, IEEE*, Balaji V. Venkatasubramanian, *Senior Member, IEEE*, Pierluigi Mancarella, *Fellow, IEEE*, and Mathaios Panteli, *Senior Member, IEEE*

Abstract—Power grids face significant threats from severe disturbances, often triggered by extreme weather, leading to widespread cascading power outages. Although intentional controlled islanding (ICI) is an effective last-resort operational mitigation strategy employed by system operators worldwide to prevent complete cascading blackouts, the impact of large-scale disturbances, particularly weather-induced cascading outages, on when and where to implement the ICI, is neither adequately considered nor reflected in current operational decision-making standards and procedures. This paper proposes a holistic cascading-driven ICI framework that seamlessly integrates advanced weather-related event modelling and cascading risk quantification of high-impact low-probability (HILP) (or tail-risk) events by using a novel ICI based on decision-making mechanism for enhancing the power grid operational resilience. The proposed framework provides a portfolio of mitigation actions proportional to cascading impacts, differentiating between tail-risk events and expected (average) events typically addressed in reliability-oriented studies and current industry practices, while being tailored to both near-real-time operations and short-term operational planning. The proposed framework involves system splitting around black-start units while forming stable and self-sufficient islands, thereby enhancing reliability and resilience. Studies on the IEEE 39-bus and IEEE 118-bus systems demonstrate the effectiveness with a significant improvement in served demand across all simulated initiating events, including up to $N-6$ contingencies.

Index Terms—Cascading failure, intentional controlled islanding (ICI), resilience, blackout, black-start tail-risk event.

I. INTRODUCTION

MODERN power grids are increasingly vulnerable to cascading failures driven by the rising frequency of

extreme weather events. Such failures stem from dependent component outages, often initiated by severe disturbances and amplified by protection relay operations, ultimately weakening the power grid and leading to costly blackouts [1]. Mitigating such phenomena requires remedial actions such as controlled islanding, which complements infrastructure-based measures by enhancing operational resilience [2]. Effective application of such actions depends on detailed modeling of system responses during the initiation and propagation of cascading failures. Cascading failure analysis has been widely studied through various models including topological [3], stochastic [4], statistical [5], quasi-steady state (QSS) [6], dynamic [7], and other interdependent models [8]. These models, whether stochastic or deterministic, capture the complex mechanisms of cascading failures. Metrics such as the number of affected elements and operating protection relays are essential for quantifying the impacts and informing mitigation strategies (MSs) including load reduction (LR) and controlled islanding.

Controlled islanding, or intentional system partitioning, is a last-resort remedial action designed to confine cascading failures and limit blackout severity. By isolating the affected section from the healthy network, it suppresses the initiating events locally and thereby enhances resilience, particularly against weather-related disturbances. Formulations of controlled islanding typically employ graph theory [9], clustering techniques [10], or linear/nonlinear programming [11], individually or in hybrid forms. Recent studies also incorporate artificial intelligence techniques such as genetic algorithms [12], grey wolf optimized neural networks [13], particle swarm optimization [14], and ant colony methods [15]. The intentional controlled islanding (ICI) problem is inherently a constrained combinatorial optimization task, aiming to minimize the power flow disruption, power imbalance, load shedding, and voltage and frequency deviations.

Depending on the time frame and type of MSs against the spread of anticipated or evolving events, ICI can be considered either preventive [11], [12] or corrective [16], [17]. Preventive ICI, implemented ahead of anticipated events, involves actions such as generator rescheduling and demand response. Corrective ICI is applied after disturbances and rely on rapid measures including load curtailment and frequency reserve activation. From a resilience perspective, several studies have proposed advanced methods. Reference [18] in-

Manuscript received: December 21, 2024; revised: April 23, 2025; accepted: September 19, 2025. Date of CrossCheck: September 19, 2025. Date of online publication: October 15, 2025.

This work was supported in part by H2020 and Horizon Europe program through the projects “HVDC-based Grid Architectures for Reliable and Resilient Wide Spread Hybrid AC/DC Transmission Systems” (HVDC-WISE) (No. 101075424), “Reliability, Resilience, and Defense Technology for the Grid” (R2D2) (No. 101075714), and “EUniversal” (No. 864334).

This article is distributed under the terms of the Creative Commons Attribution 4.0 International License (<http://creativecommons.org/licenses/by/4.0/>).

S. Hashemi (corresponding author), B. V. Venkatasubramanian, and M. Panteli are with the KIOS Research and Innovation Center of Excellence, University of Cyprus, Nicosia 1678, Cyprus (e-mail: hashemi.seyedsina@ucy.ac.cy; venkatasubramanian.balaji@ucy.ac.cy; panteli.mathaios@ucy.ac.cy).

P. Mancarella is with The University of Melbourne, Melbourne, Australia, and he is also with The University of Manchester, Manchester, UK (e-mail: pierluigi.mancarella@unimelb.edu.au).

DOI: 10.35833/MPCE.2024.001371



corporates transient stability constraints, while [19] emphasizes frequency stability. Reference [12] develops a preventive scheme for typhoon events using the Batts model and fragility curves. Data-driven detection based on wide-area measurements is proposed in [20], while [21] introduces a hybrid optimization method balancing disruption and stability with efficient black-start allocation. A three-stage cutset optimization method is presented in [22], and [23] applies genetic algorithms to manage temporary over-voltages and distributed generation utilization. Finally, [24] proposes a control strategy of microgrid to enhance resilience through coordinated energy sharing and frequency support.

Operational standards provide guidance on managing large-scale disturbances but lack explicit frameworks for controlled islanding. The ENTSO-E Operation Handbook [25], [26] emphasizes system security, incident containment, and coordinated restoration, aligning with resilience principles. IEEE Standard 1547-2018 [27] specifies requirements for both unintentional and intentional islanding, focusing on stability and distributed energy resource (DER) transitions. North American Electric Reliability Council (NERC) EOP-011-1 and EOP-011-2 [28], [29] address emergency preparedness, while independent system operator (ISO) New England OP-19 [30] provides transmission operation procedures during emergencies. However, none of these documents define controlled islanding strategies to prevent or mitigate cascading failures, which is a critical gap for resilience under extreme events.

Most existing studies [18], [19] evaluate islanding under a limited set of random $N-k$ contingencies, often neglecting the timescales of mitigation and the cascading impacts of weather-related events. As a result, their strategies may be inefficient under uncertain conditions. To address this gap, this paper proposes a holistic cascading-driven ICI framework that integrates reactive and proactive measures, tailored to event type, operating condition, and severity of cascading failures. The proposed framework combines quantification, detection, and mitigation of cascading failures, identifies assets vulnerable to windstorms, and evaluates their impacts in order to guide operational responses. By managing multiple concurrent outages including events up to $N-k$ contingencies, the proposed framework systematically enhances resilience against both expected and high-impact low-probability (HILP) events. Designed for both short-term operational planning and near-real-time operation, it explicitly accounts for stochastic weather-driven disturbances.

Indeed, the novelty of this paper lies in integrating several key modules into the proposed framework that enables system operators to make informed decisions for mitigating the impacts of cascading failures, which is an increasingly critical need in light of recent large-scale blackouts such as the one in the Iberian Peninsula. Central to the proposed framework is the decision-making mechanism that leverages cascading quantification metrics to determine the appropriate MS, thereby addressing the “when” aspect of ICI. Based on this, the optimization problem of ICI is formulated, enhanced by an inno-

vative search space reduction (SSR) technique, to deliver optimal solutions that address the remaining ICI objectives of “where” and “how” to execute system partitioning effectively, with a particular focus on maintaining post-islanding stability. The main contributions of this paper are outlined as follows.

1) A holistic cascading-driven ICI framework is proposed by capturing impacts of cascading failures and enabling zonal restoration through the assignment of black-start units (BSUs) to islands.

2) The risks of weather-induced cascading failures are quantified, where triggering events are spatially correlated by employing a stochastic spatiotemporal weather event simulator and QSS cascading failure analysis.

3) The benefits of a portfolio of mitigation actions are demonstrated and quantified, enabled by fast and reliable ICI based on the decision-making mechanism, guided by cascading failure analysis for enhancing power grid operational resilience, and tailored to timescales, operating conditions, and severity of cascading failures.

4) ICI solutions are provided that address “when”, “where”, and “how” to island based on cascading impacts, by identifying optimal island networks around coherent generator groups (CGGs), ensuring stability after boundary lines are opened.

The remainder of this paper is organized as follows. Section II presents a detailed overview of the proposed framework. Section III delves into simulation studies and results for a large set of both deterministic and stochastic contingencies. Finally, Section IV concludes this paper.

II. PROPOSED FRAMEWORK

A. Illustration of Proposed Framework

Figure 1 illustrates the proposed framework for enhancing power grid operational resilience, which is applicable to both short-term operational planning and near-real-time operation. The proposed framework addresses weather- and non-weather-related events, particularly HILP events, through MSs that mitigate cascading failures. It supports both proactive and reactive applications, as represented by the resilience trapezoid curve [31]. In operational planning, preventive ICI can be implemented hours ahead using projected data, isolating vulnerable areas to limit the propagation of cascading failures and reduce demand loss. In the near-real-time application, corrective ICI mitigates the evolving events based on current data. As shown in Fig. 1, corrective ICI typically results in greater degradation, as the occurrence of an early event triggers additional element tripping and load shedding before islanding is implemented. Preventive ICI, by contrast, reduces degradation by allowing operators to redispatch generation, adjust topology, and implement the LR ahead of time.

Figure 2 presents the detailed flowchart of the proposed framework, which incorporates the cascading failure analysis module, resilience assessment and decision-making module, and MS module. The event simulator, cascading failure modeling, resilience assessment, decision-making, and ICI are integrated into a unified framework.

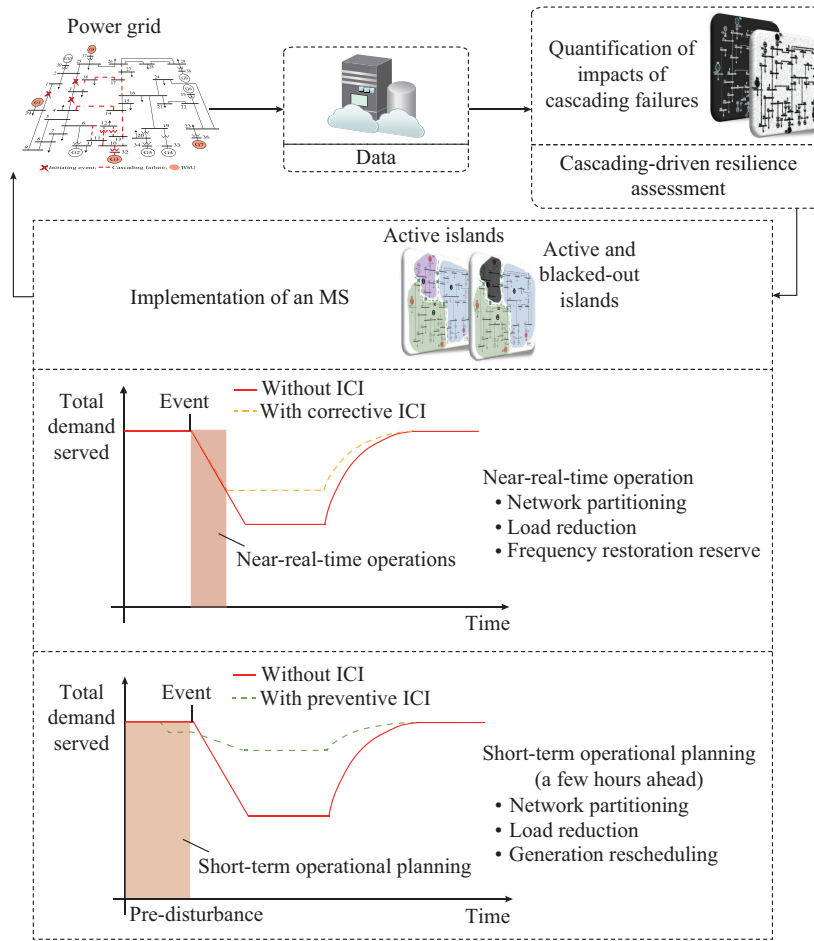


Fig. 1. Illustration of proposed framework for enhancing power grid operational resilience.

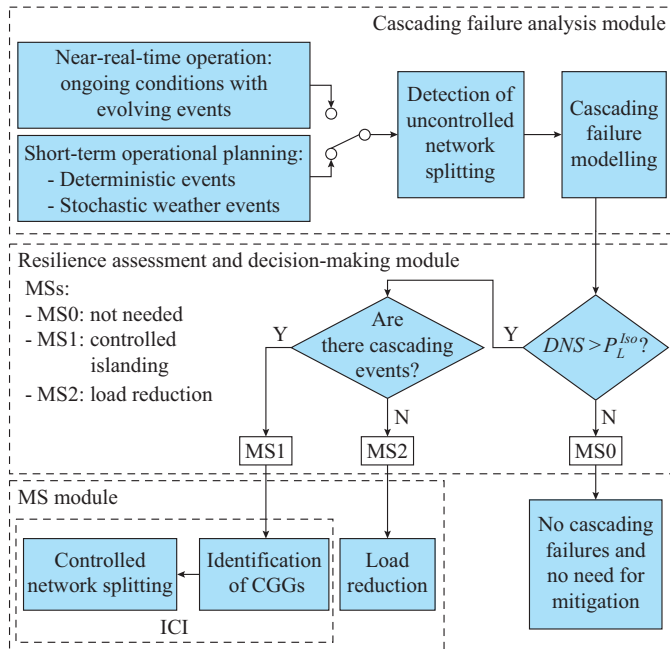


Fig. 2. Detailed flowchart of proposed framework.

This integration is one key novelty of this paper, enabling operators to make informed decisions for mitigating the impacts of cascading failures. In Fig. 2, DNS represents the de-

mand not served (DNS); and P_L^{Iso} is the interrupted load from isolated buses.

The process begins with resilience assessment through modeling and quantification of cascading failures. Inputs include specific initiating events for near-real-time operation or wind event-based scenarios for short-term operational planning. Two metrics are employed: DNS to characterize cascade size and the number of affected components to indicate grid integrity. Based on these metrics, the decision-making module selects the appropriate MS. If events do not propagate under controlled LR, curtailment is applied proportionally across loads; otherwise, ICI is executed. For cascading failure modeling, the proposed framework employs the AC-cascading failure modelling (CFM) method [6], which integrates AC power flow and QSS calculations to assess system performance under disturbances. Inputs are provided either by the event simulator, which generates anticipated weather-related and $N-k$ contingency scenarios for short-term planning, or by observed initiating events in near-real-time operation.

This comprehensive setup for the proposed framework enables cascading quantification and supports the selection of MSs, effectively addressing the three key objectives of ICI: when, where, and how to island. The “when” objective is determined by resilience assessment and decision-making mod-

ule, which evaluates whether triggering events initiate a propagating cascade or remain contained. If propagation is confirmed, ICI is applied to define “where” boundary lines should be opened and “how” to maintain stability and self-sufficiency across the resulting islands.

System splitting may be accompanied by generation re-scheduling, utilization of frequency reserve, and LR within islands that are experiencing imbalance between load and generation. In this paper, the objective is to minimize the total system DNS resulting from load-generation imbalances, as formulated by (1).

$$\min \zeta_k \left[\sum_{j \in \mathcal{A}_k} x_j P_{L,j} - \sum_{i \in \mathcal{Q}_k} x_i (P_{g,i} + FRR_{g,i}) \right] \quad k \in K \quad (1)$$

$$\zeta_k = \sum_{m \in B_{Isl_k}} \underline{Z}_m \quad (2)$$

where K is the set of controlled islands; ζ_k is the total impedance-based distance in island k ; $P_{L,j}$ is the active power of load j ; \mathcal{A}_k is the set of load buses in island k ; $P_{g,i}$ and $FRR_{g,i}$ are the active power and frequency restoration reserve (FRR) of generator i , respectively; \mathcal{Q}_k is the set of coherent generators in island k ; \underline{Z}_m is the shortest impedance-based distance from bus m to CGGs of island k , and is calculated as the smallest length of the path between two nodes using the Dijkstra algorithm [32]; and B_{Isl_k} is the set of buses in island k . The problem is constrained by two sets of constraints: structural and operational, which are further detailed in Section II-D-2).

B. Resilience Assessment

This subsection assesses the resilience of a disturbed power grid. The disturbances may include specific initiating events that have already taken place or anticipated weather-related events, depending on the timescales of the mitigative measures. This paper utilizes the wind event modelling developed in [33] for resilience assessment, extending beyond the deterministic $N-k$ ($k \in [1, 3]$) contingencies.

1) Event Simulator

The event simulator generates $N-k$ transmission line contingencies deterministically ($k \in [1, 3]$) or stochastically ($k > 3$). A fragility-based wind event model is employed to anticipate line outages from upcoming weather incidents. The resulting operating conditions are then analyzed using quasi-steady-state cascading failure modeling for short-term operational planning (see Fig. 2). Fragility curves, derived from statistical, experimental, simulation-based, or expert methods, define the probability of line failure as a function of hazard intensity. By following [33], wind-dependent fragility curves are applied to model line outages. Windstorm characteristics such as gust speed and radius are extracted from historical data [34], [35], and Monte Carlo simulations generate a large set of stochastic scenarios. By varying storm parameters, the simulator captures uncertainty and determines line outage status LS , with tripping decisions based on (3).

$$LS(w_{st}, l) = \begin{cases} 1 & \mathcal{P}_l(w_{st}) < r \\ 0 & \mathcal{P}_l(w_{st}) \geq r \end{cases} \quad (3)$$

where w_{st} is the wind intensity or wind speed at step st ; \mathcal{P}_l is the wind-dependent failure probability of line l ; and r is the random number generated between 0 and 1. The concept of r is introduced to add more stochasticity to the model.

2) Detection of Uncontrolled Network Splitting (UNS)

Depending on the severity and number of concurrent initiating events, particularly weather-related events that are spatially correlated and capable of simultaneously disrupting nearby transmission lines, early UNS including the isolation of at least one load bus is highly likely to occur, as conceptually shown in Fig. 3.

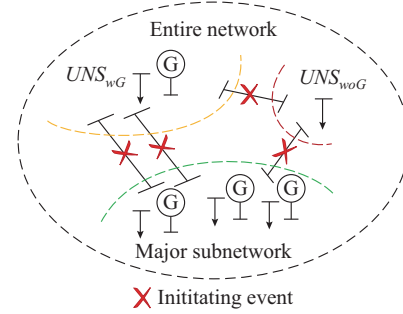


Fig. 3. Detection of UNS caused by initiating events.

To detect UNS and integrate it into the proposed framework, Algorithm 1 is developed. In this paper, UNS involves isolated buses B_{iso} , either without generation (denoted by UNS_{woG}) or with at least one generator (denoted by UNS_{wG}). As UNS_{woG} inevitably experiences outages, the focus is on the remaining network. Each UNS_{wG} is treated as a minor subnetwork, while the rest forms the major subnetwork, both potentially requiring ICI depending on size and severity of cascading failures. If B_{iso} contains both load and generator buses, it is classified as UNS_{wG} . Since splitting can fragment the network into multiple segments that contain generators, each UNS_{wG} is analyzed individually as a minor subnetwork in Algorithm 1. The decision-making indicator I_{DM}^{mn} then specifies whether ICI is required or not, denoted by 1 and 0, respectively. In Algorithm 1, \mathcal{A} is the set of isolated buses; B_G is set of generator buses; N_{minor} is the set of minor subnetworks; N_{Isl}^{UNS} is the number of islands in an isolated subnetwork; and DNS^{mn} is the DNS of minor subnetwork.

The number of islands N_{Isl} is calculated using (4) based on the number of BSUs N_{BSU} and the total number of buses N . The formulation ensures that each partitioned network is sufficiently large, defined as $\lfloor 0.5\sqrt{N} \rfloor$ [36], and contains at least one BSU. If N_{Isl}^{UNS} exceeds two, ICI may be applied, with the decision-making indicator I_{DM}^{mn} set to be 1. Otherwise, I_{DM}^{mn} is set to be 0, and stability must be preserved through LR, frequency reserves, or generation rescheduling. Minor subnetworks with less than two islands are excluded from ICI, while isolated buses without generation experience blackout. The outputs include P_L^{iso} , DNS^{mn} , and data for both minor and major subnetworks.

Algorithm 1: detection of UNS

Detect isolated buses B_{iso}
if $\exists B_{iso} \in A$ **then**
 if $\exists B_{iso} \in B_G$ **then**
 $UNS_{wG} \subseteq N_{minor}$
 if $N_{isl}^{UNS} \geq 2$ (as per (4)) **then**
 Quantify DNS^{mn} using CFA of the UNS, and $I_{DM}^{mn}=1$ (ICI may be needed)
 else
 Quantify DNS^{mn} using CFA of the UNS, and $I_{DM}^{mn}=0$ (no need for ICI but LR may be needed)
 end if
 else
 Calculate P_L^{Iso} for buses with load but without a generator
 end if
else
 $P_L^{Iso}=0$ for buses with neither load nor a generator
end if

$$N_{isl} = \min \left(N_{BSU}, \left\lfloor 0.5 \sqrt{N} \right\rfloor \right) \quad (4)$$

3) Modelling and Quantification of Cascading Failures

Resilience assessment is performed using QSS cascading failure modeling, specifically in the AC-CFM method [6]. This fast recursive method simulates the successive activation of protection mechanisms and models cascading failure that may propagate within each island. It incorporates overload protection (OLP), under-frequency load shedding (UFLS), over-frequency generator shedding (OFGS), under-voltage load shedding (UVLS), and generator over/under-excitation limiters (O/UXLs), enabling replication of steady-state frequency and voltage responses. The power flow redistribution after component failures is captured, leading to overloads (OLs) and line tripping. The impacts of cascading failures are quantified through metrics such as DNS and the number of affected elements. These results inform the decision-making module, in which the appropriate MS is selected.

C. Decision-making Mechanism for MS

Based on the cascading-driven feature of the proposed framework shown in Fig. 2, the decision-making mechanism determines when to island based on assessed cascading risks and what-if analysis. It evaluates cascading initiation and propagation using two metrics: cascade size, measured as DNS, and grid integrity, quantified by the number of tripped elements N_{TE} . DNS reflects protection actions such as under-voltage and under-frequency load shedding, while N_{TE} captures effects of overcurrent relay operations and generator tripping. Although simple, the decision-making mechanism is robust, relying on the current operating conditions and cascading failure analysis using AC power flow and QSS calculations. Decisions are made quickly through threshold rules derived from these analyses.

Algorithm 2 defines the decision-making mechanism, which selects the most effective MS based on cascading severity, load isolation, ICI, or LR. The decision-making indicator I_{DM}^{MS} takes values of 0, 1, or 2, corresponding to load isolation, ICI, or LR, respectively. If DNS in either the ma-

ior network DNS^{MN} or minor subnetwork DNS^{mn} (with $I_{DM}^{mn}=1$) exceeds zero and the cascading propagation is confirmed ($N_{TE}>0$), ICI (denoted by MS1) is triggered. If no propagation occurs ($N_{TE}=0$), LR (denoted by MS2) suffices to alleviate stress and halt the cascade. These rule-based decisions, formulated in (5), precede the optimization-based ICI process. In controlled LR, the reduction is proportional to the share of the total connected load. Otherwise, if ICI is required, the corresponding optimization problem is solved. The decision is expressed as:

$$\text{Decision} = \begin{cases} \text{No action} & DNS < P_L^{Iso} \\ \text{LR} & DNS > P_L^{Iso} \text{ and } N_{TE} = 0 \\ \text{ICI} & DNS > P_L^{Iso} \text{ and } N_{TE} > 0 \end{cases} \quad (5)$$

Algorithm 2: decision-making mechanism for MS

Update the data from the available network elements
Identify the minor and major subnetworks using Algorithm 1
Update the total amount of P_L^{Iso} and DNS^{mn} after initiating events
Quantify DNS^{mn} using CFA performed for the remaining active network or major subnetwork, $DNS = DNS^{MN} + DNS^{mn} + P_L^{Iso}$
if $DNS^{MN} > 0$ or ($DNS^{mn} > 0$ and $I_{DM}^{mn} = 1$) **then**
 if any subsequent cascading outages occur ($N_{TE} > 0$) **then**
 Need to halt cascading propagation by performing MS1, $I_{DM}^{MS} = 1$
 else
 Perform LR per bus to control the system and satisfy operational constraints (MS2), $I_{DM}^{MS} = 2$
 end if
else
 Perform load interruption due to bus isolation (no cascading occurs), $I_{DM}^{MS} = 0$
end if

D. MS

The MS pointed out in Algorithm 2, which involves LR and ICI based on the impacts of initiating events and subsequent cascading events, are detailed in this subsection.

1) LR

In essence, LR limits customer demand in targeted areas or across the entire system through operator-directed control actions or automated protective load-shedding schemes. Beyond balancing supply and demand to maintain the frequency stability, it mitigates cascading propagation by relieving stress from post-event power flow redistribution. When triggered by the decision-making module (MS2), LR addresses the line OL and imbalance between load and generation. Depending on the timescale, it may be combined with generation rescheduling in short-term operational planning or frequency reserve utilization in near-real-time operation. Curtailment is allocated proportionally to the share of total demand for each load. For the test system, LR is quantified using (6), which incorporates generator contributions to the FRR, yielding the total reduction for island k LR_k . In short-term operational planning, $FRR_{g,i}$ is zero, but $P_{g,i}$ may change due to generation rescheduling. In contrast, in near-real-time operations, $P_{g,i}$ remains unchanged, while $FRR_{g,i}$ varies.

$$LR_k = \sum_{j \in A_k} P_{l,j} - \sum_{i \in \Omega_k} (P_{g,i} + FRR_{g,i}) \quad (6)$$

2) ICI

The ICI determines where and how to island by forming stable, self-sufficient islands around BSUs. Using system data and outputs from the resilience assessment and decision-making module, it identifies boundary buses and lines while maintaining the frequency and rotor angle stability through coordinated load and generation control.

1) Identification of CGG

To preserve rotor angle stability after ICI, CGGs must be identified. Algorithm 3 outlines this process using terminal voltage phase angles of generator from the PMUs [11]. Coherency is quantified through the intraclass correlation coefficient (ICC), scaled from 0 to 1, and weighted by impedance-based electrical distances to ensure spatial proximity and avoid infeasible partitions. A K -medoids spectral clustering algorithm [37] is then applied to the distance-weighted ICC (DICC) values using 100 samples of 10 ms, each within a moving window. Electrical distance is defined as the minimum equivalent impedance between generators and computed via the Dijkstra algorithm [32]. The DICC formulation is given in (7).

Algorithm 3: identification of CGGs

Update the data from the available network elements
 Calculate the sparse impedance matrix of the network Z_{bus}
 Establish impedance-weighted graph of the power grid
for $i \in B_G$ **do**
 for $j \in B_G$ **do**
 if $i \neq j$ **then**
 Calculate $IBD_{i,j}$ by finding the shortest length $\mathbb{L}(\mathbb{P})$ among the paths between the origin generator node i and the destination node j using the Dijkstra algorithm (see (8))
 Calculate the ICC between each pair of phase angles $ICC_{i,j}$
 Calculate DICC between each pair of phase angles $DICC_{i,j}$ (see (7))
 else
 $DICC_{i,j} = 1$
 end if
 end for
end for
 Identify coherent groups of generators around BSUs using K -medoids clustering algorithm based on $DICC_{i,j}$

$$DICC_{i,j} = 1 - \left[IBD_{i,j} \odot (1 - ICC_{i,j}) \right] \quad \forall i, j \in B_G \quad (7)$$

where $IBD_{i,j}$ is the impedance-based distance between each pair of generators (i, j); $ICC_{i,j}$ is the ICC of the phase angles for each pair of generators; $DICC_{i,j}$ is the DICC of generators ranging from 0 to 1, with values closer to 1 indicating greater coherency; and \odot denotes the element-wise product operation. $IBD_{i,j}$ is calculated by finding the shortest length $\mathbb{L}(\mathbb{P})$, where \mathbb{P} is the path between each pair of generators (i, j) in the impedance-weighted graph of power grid $\mathcal{G} = (\mathbb{V}, \mathbb{E}, \mathbb{W})$, where \mathbb{V} is the set of vertices, \mathbb{E} is the set of edges, and \mathbb{W} is the weight associated with the edges in graph \mathcal{G} .

$$IBD_{i,j} = \min \mathbb{L}(\mathbb{P}_{i,j}: i \rightarrow j) \quad \forall i, j \in B_G \quad (8)$$

This calculation is updated dynamically after cascading quantification, resilience assessment, and decision-making, capturing near-real-time changes such as outages or imped-

ance variations for use in ICI. To ensure the presence of BSUs, they serve as central cores in CGG identification, and the availability is rechecked. The number of CGGs, equivalent to the required islands for cascading-driven partitioning, is determined by (4) (Section II-B-2)). The resulting set $GCG_\gamma, \gamma \in K = \{1, 2, \dots, k, \dots, N_{Isl}\}$ is expressed in (9).

$$CGG = \{GCG_\gamma | \gamma \in K\} \quad (9)$$

2) Controlled network splitting

The ICI based on decision-making mechanism reduces computational burden by limiting search space (SS) using electrical distance. As outlined in Algorithm 4, buses close to a CGG are directly assigned to that island and excluded, while marginal buses, which are nearly equidistant or located at boundaries, define the reduced SS. The solver then operates on this subset to identify optimal boundary buses for islanding.

Algorithm 4: cascading-driven ICI framework

Update the data of the minor and major subnetworks
if $I_{DM}^{MS} = 1$ **then**
 Identify the marginal buses
 Run the subroutine of Algorithm 3 to identify CGGs
 while stopping criterion is unmet **do**
 Solve the optimization problem subject to all constraints (find a set of decision variables that minimizes the objective function while satisfying all constraints)
 end while
end if
 Identify all islands and update their corresponding networks
 Calculate the total value of DNS for entire network: $DNS = \sum_k DNS_k^{Isl} + P_L^{Iso}$
return DNS, the boundary lines, the set of buses pertaining to each island, and load and generation values at each bus

In this paper, the SSR technique is innovatively introduced for the ICI, which applies impedance-based electrical distance to limit possible solutions. Since assigning buses far from reactive power sources can bring risks of voltage instability, subnetworks are first formed around CGGs using shortest-path distances. Buses near island boundaries are then identified as marginal buses, determined by their maximum impedance-based distance to CGGs. These marginal buses define the SS of the problem, which is explored by an optimization algorithm to minimize the imbalance between load and generation. The process is conceptually illustrated in Fig. 4.

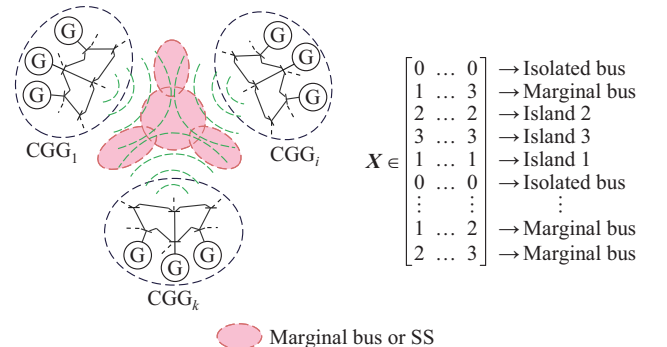


Fig. 4. Process of SSR technique involving marginal or distant buses.

Following the initiating events, the topological integrity of the system is first assessed. If unintentional splitting occurs, the isolated minor subnetwork is excluded from the islanding, with its decision variables set to be zero. For the remaining major subnetwork, bus decision variables take integer values ranging from 1 to N_{Isl} , representing island assignments. As formulated in (10), buses are allocated to islands based on their shortest distance to the corresponding CGG, while marginal buses at boundaries may take any island value from the set K .

$$x_i = \begin{cases} k & i \in B_{Isl_k} \\ K_i & i \in B^{Marg} \\ 0 & \text{otherwise} \end{cases} \quad (10)$$

where B^{Marg} is the set of marginal buses with $B^{Marg} \subset B^{MmN}$, and B^{MmN} is the set of buses belonging to the major and minor subnetworks; B_{Isl_k} is a subset of B^{MmN} , and x_i is the decision variable for bus i that takes the value of the island number k if it has the shortest distance to the CGG of island k . The decision variables for the marginal buses around the boundary of the islands can take integer values from the set K representing the island numbers (see Fig. 4).

As a result of the SSR technique, two vectors for the lower and upper bounds of the decision variables are calculated, as formulated in (11).

$$X = [x_i]_{i \in B^{MmN}} \in [\underline{X}, \bar{X}] \quad (11)$$

The problem solver only needs to search the space within these bounds to find an optimal solution for the boundary buses and the lines connecting each pair of islands. As illustrated in Fig. 4, and assuming that there are three islands, the decision variable X lies within bounds \underline{X} and \bar{X} , taking integer values from 0 to 3. A value of 0 denotes an isolated bus, while other integers assign buses to the corresponding island based on shortest distance (e.g., 2 for Island 2). Marginal bus assignments, boundary line identification, and the optimal post-islanding operating point are determined by solving the optimization problem in (1). The resulting subnetworks are then updated to reflect the optimal ICI solution.

The structural constraints ensure the network connectivity and the assignment of at least one BSU to each island, facilitating the restoration of a blackout island after an ICI failure. Equation (12) ensures that every bus i with a non-zero decision variable $x_i \neq 0$ in B^{MmN} is assigned to a specific island, thereby maintaining connectivity within the subnetwork of islands without isolated buses after ICI. $|B^{MmN}|$ denotes the cardinality (or size) of set B^{MmN} . Equation (13) ensures that for each $\gamma \in K$, there is at least one BSU_i in CGG_γ . The binary variable $u_{i,\gamma}$ takes the value 1 if BSU_i is in CGG_γ , and 0 otherwise.

$$\frac{1}{x_i} \sum_{i \in B^{MmN}} x_i = |B^{MmN}| \quad x_i \neq 0, \forall i \in B^{MmN} \quad (12)$$

$$\sum_{i \in BSU} u_{i,\gamma} \geq 1 \quad \forall \gamma \in K \quad (13a)$$

$$u_{i,\gamma} = \begin{cases} 1 & BSU_i \in CGG_\gamma \\ 0 & \text{otherwise} \end{cases} \quad (13b)$$

The constraints ensure that all operating limits are met, including line power flow (14)-(19), generator active and reactive power (17), (18), and bus voltage (19). During optimization, if a constraint is violated, LR and generation rescheduling are implemented to find a feasible and optimal solution.

$$P_{ij} = G_{ij}V_i^2 - V_iV_j(G_{ij} \cos \theta_{ij} + B_{ij} \sin \theta_{ij}) \quad \forall (i,j) \in B_{line} \quad (14)$$

$$Q_{ij} = V_iV_j(G_{ij} \sin \theta_{ij} - B_{ij} \cos \theta_{ij}) - G_{ij}V_i^2 \quad \forall (i,j) \in B_{line} \quad (15)$$

$$\sqrt{P_{ij}^2 + Q_{ij}^2} \leq \bar{S}_{ij} \quad \forall (i,j) \in B_{line} \quad (16)$$

$$\underline{P}_{Gi} \leq P_{Gi} \leq \bar{P}_{Gi} \quad \forall i \in B_G \quad (17)$$

$$\underline{Q}_{Gi} \leq Q_{Gi} \leq \bar{Q}_{Gi} \quad \forall i \in B_G \quad (18)$$

$$\underline{V} \leq V_i \leq \bar{V} \quad \forall i \in B \quad (19)$$

where P_{ij} , Q_{ij} , and \bar{S}_{ij} are the active, reactive, and maximum apparent power flows of line ij , respectively; V_i and V_j are the voltages of buses i and j , respectively; G_{ij} and B_{ij} are the conductance and admittance of line ij , respectively; θ_{ij} is the voltage angle; P_{Gi} and Q_{Gi} are the active and reactive power of generator bus, respectively; \underline{P}_{Gi} , \bar{P}_{Gi} and \underline{Q}_{Gi} , \bar{Q}_{Gi} are the lower and upper bounds of P_{Gi} and Q_{Gi} , respectively; \underline{V} and \bar{V} are the lower and upper bounds of V_i , respectively; B is the set of buses; and B_{line} is the set of two-end pair buses of lines.

The voltage and reactive power constraints accommodate voltage deviations within permissible operating limits at post-islanding operating points, while the objective function of minimizing the imbalance between load and generation helps mitigate frequency deviations. Together, these elements significantly ensure the post-islanding stability and align with the ‘‘how’’ objective of the ICI.

III. SIMULATION STUDIES AND RESULTS

The IEEE 39-bus system (345 kV with 6254.2 MW total load) is used to evaluate the proposed framework. The optimization problem is solved with the MATLAB mixed-integer nonlinear toolbox [38] and MATPOWER [39]. Simulation is performed on a PC with an Intel Core i7 (2.8 GHz, 16 GB RAM), yielding an average computation time of around 15 s across all scenarios for the test system. Generators are assumed to provide up to 5% of capacity as frequency restoration reserves [40], and all transmission lines are considered available for de-energization to enable the islanding. BSUs are located at buses 32, 36, 37, and 39. The proposed framework is tested for both near-real-time operation, addressing the evolving events and short-term operational planning, and covering weather- and non-weather-related events.

A. Near-real-time Operation Under Evolving Events

In this case, three lines (1-39, 2-3, and 3-4) are removed for initiating events (denoted by ‘‘EV’’ in Fig. 5(b)), representing an $N-3$ contingency. This outage set does not cause early isolation of bus or minor subnetworks ($P_L^{iso}=0$, $I_{DM}^{mn}=0$). Cascading failure analysis shows propagation with

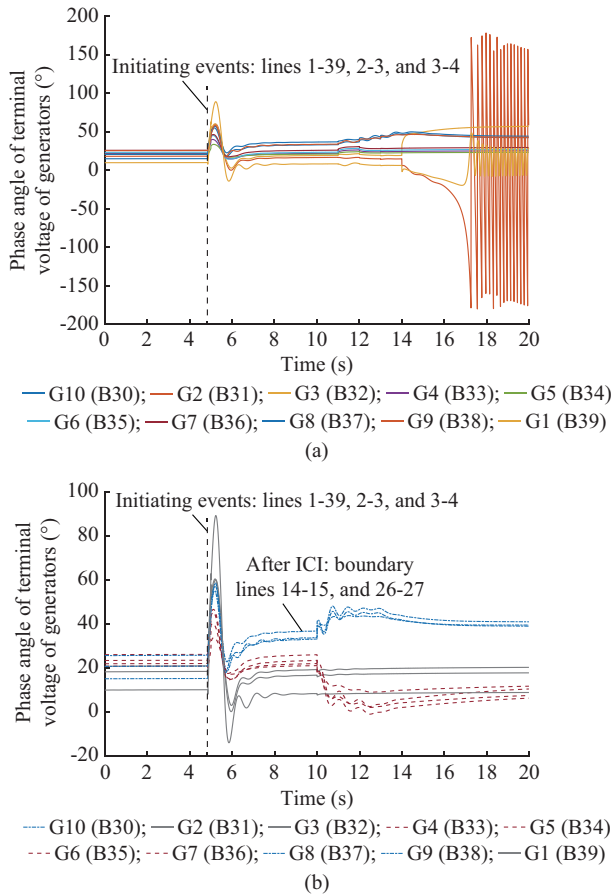


Fig. 7. Phase angles of terminal voltages of generators. (a) Before ICI. (b) After ICI.

Another instance of initiating events, representing an extreme weather-related event, considers outages of lines 1-2, 1-39, 2-3, 2-25, 17-18, and 17-27, creating a minor isolated subnetwork. Figure 8(a) highlights the wind-affected region of the system by means of a purple dashed arrow and a purple circular marker.

Generated by the event simulator with stochastic $N-k$ contingencies ($k \in [1, 6]$), this event forms isolated buses 1, 2, 30, and a minor subnetwork (with buses 25-29, 37, 38). As detailed in Section II-B-2), since $N_{IsI} < 2$, this subnetwork is excluded from ICI and mitigated with LR only. The initial interruption of load due to isolation of bus 1 and the DNS before implementing ICI are $P_L^{iso} = 97.6$ MW and $DNS = 2170.35$ MW, respectively. The major subnetwork is then split by opening line 14-15, reducing the DNS to 726.5 MW (a 66.5% improvement in served load), as shown in Fig. 8(b).

B. Short-term Operational Planning for Weather- and Non-weather-related Events

The proposed framework is evaluated under extreme uncertain conditions, including severe weather- and non-weather-related events. In short-term operational planning studies for a few hours ahead, operators can assess the system under potential and anticipated events, such as deterministic $N-1$, $N-2$, and $N-3$ contingencies of transmission lines, along with a set of stochastic scenarios involving wind events.

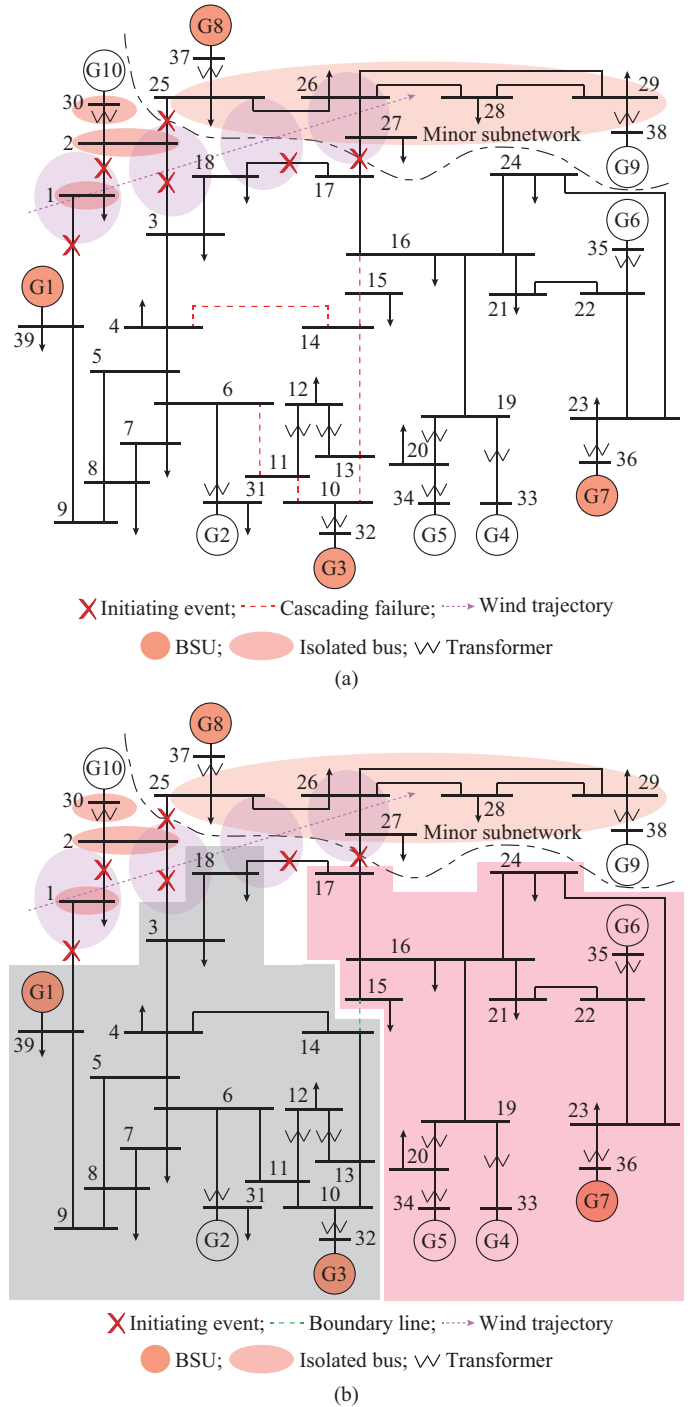


Fig. 8. CFA before and after ICI with outage of three lines. (a) Before ICI. (b) After ICI.

This subsection involves analyzing $N-k$ contingencies ($k \in [1, 3]$) of transmission lines deterministically and $N-k$ contingencies ($k \in [1, 6]$) stochastically, based on 1000 wind-related stochastic events. These stochastic events include 91, 60, and 53 distinct contingency sets for $N-4$, $N-5$, and $N-6$ contingencies, respectively. The operators can reschedule system generation during ICI due to sufficient time before events, reducing reliance on load curtailment.

Applying the same outage scenario as in Section III-A, Table I compares preventive ICI implemented through genera-

tion rescheduling and LR one and two hours ahead, with corrective ICI based on FRR and LR.

TABLE I
COMPARISON OF PREVENTIVE ICI WITH CORRECTIVE ICI

| Type of ICI | Time ahead | Remedial action | Power (MW) |
|-------------|-----------------|-------------------------|------------|
| Preventive | One hour ahead | Generation rescheduling | 696.0 |
| | | LR | 708.9 |
| | Two hours ahead | Generation rescheduling | 1392.0 |
| | | LR | 12.9 |
| Corrective | None | FRR | 117.5 |
| | | LR | 1287.4 |

The results show that proactive measures (preventive ICI) achieve greater resilience than reactive measures (corrective ICI), as illustrated in Fig. 1. Based on generator ramp rates

TABLE II
COMPARISON OF DIFFERENT MSS

| Scenario | Contingency | Line | DNS (MW) | | Improvement (%) | MS |
|----------|-------------|--|----------------|----------------|-----------------|-----|
| | | | Before ICI | After ICI | | |
| 1 | $N-4$ | 14-15, 16-17, 17-18, 17-27 | 0 | 0 | 0.0 | MS0 |
| 2 | $N-4$ | 13-14, 15-16, 16-21, 16-24 | 3140.8 (50.2%) | 1673.4 (26.8%) | 0.0 | MS2 |
| 3 | $N-4$ | 5-8, 6-7, 7-8, 8-9 | 4223.6 (67.5%) | 767.0 (12.3%) | 81.8 | MS1 |
| 4 | $N-5$ | 4-5, 6-11, 7-8, 8-9, 13-14 | 3298.9 (52.7%) | 1444.7 (23.1%) | 56.2 | MS1 |
| 5 | $N-5$ | 3-4, 5-6, 14-15, 15-16, 22-23 | 320.0 (5.1%) | 320.0 (5.1%) | 0.0 | MS0 |
| 6 | $N-6$ | 2-3, 3-4, 3-18, 17-18, 17-27, 26-27 | 761.0 (12.2%) | 761.0 (12.2%) | 0.0 | MS0 |
| 7 | $N-6$ | 4-14, 6-11, 10-11, 10-13, 13-14, 14-15 | 2171.2 (34.7%) | 894.3 (14.3%) | 58.8 | MS1 |

When $DNS=0$ (first row), no mitigation is required (MS0). For the second case (lines 13-14, 15-16, 16-21, and 16-24), LR of 1673.4 MW (MS2) alleviates the stress, preventing cascading and reducing DNS from 50.2% to 26.8%. In contrast, the outages of lines 5-8, 6-7, 7-8, and 8-9 trigger cascading and severe outages (67.5%), but with ICI (MS1), DNS is improved by 81.8%. Figure 9 illustrates the comparison of cascading impacts across various scenarios using different MSs.

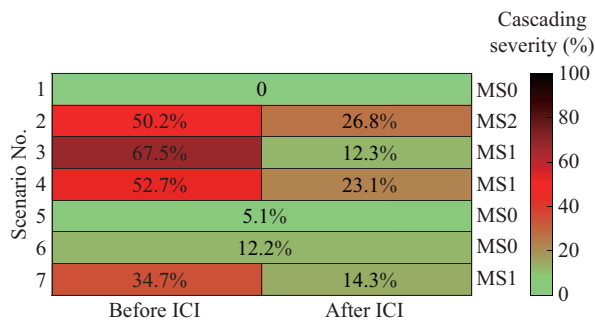


Fig. 9. Comparison of cascading impacts across various scenarios using different MSs.

Furthermore, the reliability and resilience of power grid are quantified using the expected value of DNS (EDNS) and conditional value-at-risk (CVaR) at the 95% confidence level

[42], generation rescheduling increases from 696 MW to 1392 MW, while LR decreases from 708.9 MW to 12.9 MW when implemented one and two hours ahead, respectively. As the events approach, LR requirements increase, but they overall remain lower under proactive ICI due to simultaneous generation rescheduling.

The remaining simulation assumes a one-hour-ahead horizon, with further analysis of MSs for specific extreme wind-driven events.

Table II compares different MSs (MS0, MS1, MS2) for stochastic initiating events involving the loss of 4 to 6 lines ($N-k$ contingencies, $k \in [4, 6]$), highlighting the improvement achieved after ICI compared with the state before ICI. The decision-making module selects MSs based on DNS and the number of tripped elements.

[43]. This analysis aims to demonstrate the effectiveness of proposed framework in mitigating the impact of both expected events (thereby decreasing the mean value of DNS) and the effects of unexpected tail-risk events (resulting in a reduction of the conditional values of DNS). For this purpose, $CVaR=95\%$ is considered for the average DNS among the worst 5% of events.

Table III compares the EDNS and CVaR before and after ICI for deterministic $N-k$ contingencies ($k \in [1, 3]$), showing at least 45.6% improvement in EDNS and 32.9% in CVaR for $N-3$ cases. A similar analysis of 1000 stochastic wind-related scenarios up to $N-6$ contingency demonstrates further benefits. As illustrated in Fig. 10, ICI shifts the probability distribution of DNS leftward, reducing EDNS from 1249.83 MW to 650.98 MW and CVaR from 4426.86 MW to 3241.87 MW, respectively, thereby lowering blackout risk and enhancing resilience.

TABLE III
EDNS AND CVAR BEFORE AND AFTER ICI

| Contingency | DNS before ICI (MW) | | DNS after ICI (MW) | | Improvement (%) | |
|-------------|---------------------|---------|--------------------|---------|-----------------|------|
| | EDNS | CVaR | EDNS | CVaR | EDNS | CVaR |
| $N-1$ | 753.11 | 4736.68 | 320.48 | 1975.30 | 57.45 | 58.3 |
| $N-2$ | 1317.49 | 4407.28 | 654.10 | 2860.30 | 50.35 | 35.1 |
| $N-3$ | 1745.98 | 4669.37 | 948.85 | 3133.24 | 45.65 | 32.9 |

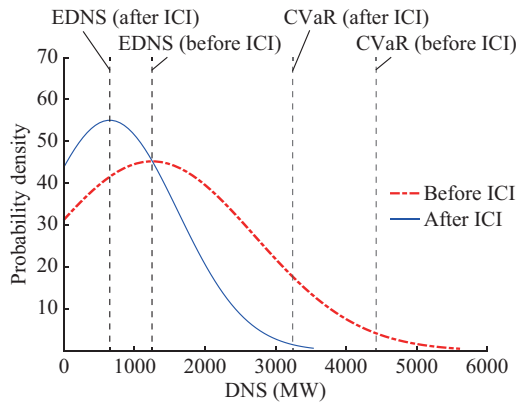


Fig. 10. PDF curves of DNS for stochastic contingencies.

To demonstrate scalability, the proposed framework is applied to the IEEE 118-bus system under initiating events of concurrent outages of lines 49-54, 59-60, 59-61, and 59-63. As shown in Fig. 11, these events trigger widespread cascading and severe blackouts.

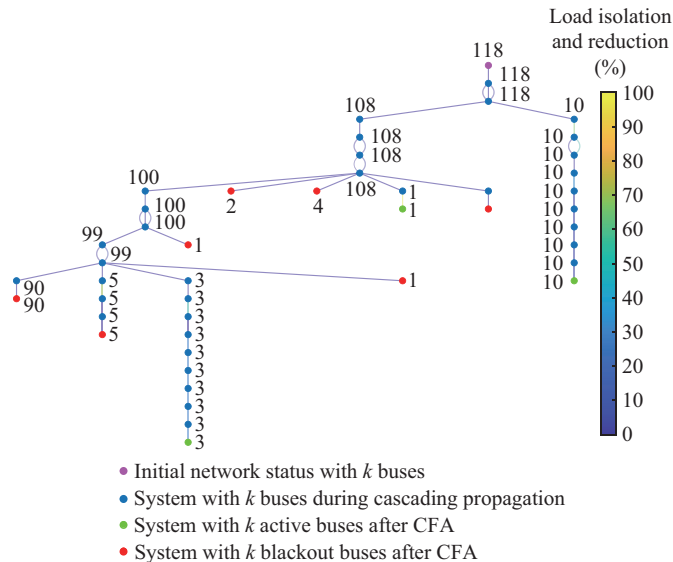


Fig. 11. Cascading failure analysis of IEEE 118-bus system under initiating events without ICI.

Figures 12 and 13 show the system frequency and voltage profile of IEEE 118-bus system under initiating events without ICI, where each cascade generation represents a stage of propagation involving tripping, load shedding, or disconnection of generator. The results show that the voltage and frequency collapse in blackout islands, while survived islands stabilize near nominal values.

Figure 14 further visualizes the impacts of cascading failures on the IEEE 118-bus system under initiating events without ICI through a node-branch graph.

Furthermore, the system performance improves remarkably with ICI. As shown in Figs. 15-18, the impacts of cascading failures are greatly reduced, and all islands stabilize with voltage and frequency near nominal values. The total computational time including cascading failure analysis, decision-making, and islanding computation is 16.4 s.

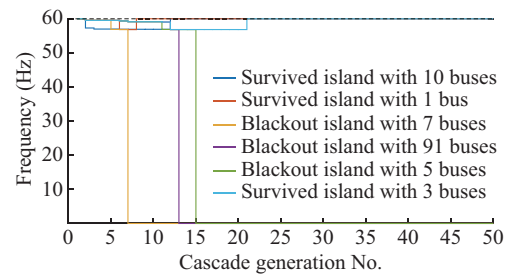


Fig. 12. System frequency of IEEE 118-bus system under initiating events without ICI.

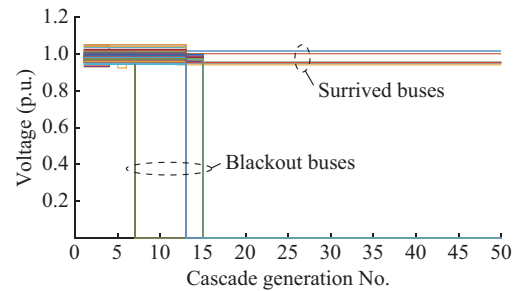


Fig. 13. Voltage profile of IEEE 118-bus system under initiating events without ICI.

Figure 19 compares the system resilience using the trapezoid curve, showing served load rising from 121.4 MW to 3960.6 MW, showing a 90.5% improvement.

C. Comparative Analysis and Validation of ICI

To benchmark the performance, the ICI is compared with the classical spectral clustering ICI (SCICI) [44], which models the power grid as a weighted graph. While computationally efficient, the SCICI addresses only the “where” objective by identifying boundary lines with minimal power flow disruption, without ensuring stable post-islanding operation (the “how” objective). The IEEE 39-bus system is reanalyzed under the same $N-3$ contingency (lines 1-39, 2-3, and 3-4) using the SCICI.

As shown in Figs. 20 and 21, the SCICI results in DNS of 1659 MW, which is higher than 1287.4 MW achieved by the ICI (Fig. 6). This difference arises because SCICI does not optimize post-islanding conditions, leading to additional relay operations. By contrast, the ICI ensures stability through optimal LR and reserve dispatch. Partitioning under SCICI is achieved by opening lines 14-15 and 25-26, as indicated by the green dashed lines in Fig. 21.

This paper further validates the ICI through dynamic simulations in DiGSILENT PowerFactory, extending beyond the QSS method. By using the same outage scenario (lines 1-39, 2-3, and 3-4 at 2 s) on the IEEE 39-bus system, the results with and without the ICI are compared.

Figure 22 shows the system load, capturing transients from controllers and relays. The DNS decreases from 1561.2 MW without the ICI to 823 MW with the ICI, confirming its effectiveness. Figure 23 illustrates the frequency responses. Without the ICI, the cascading begins at approximately 35 s, creating unstable islands at different frequencies, while with the ICI, the power grid splits into three stable islands.

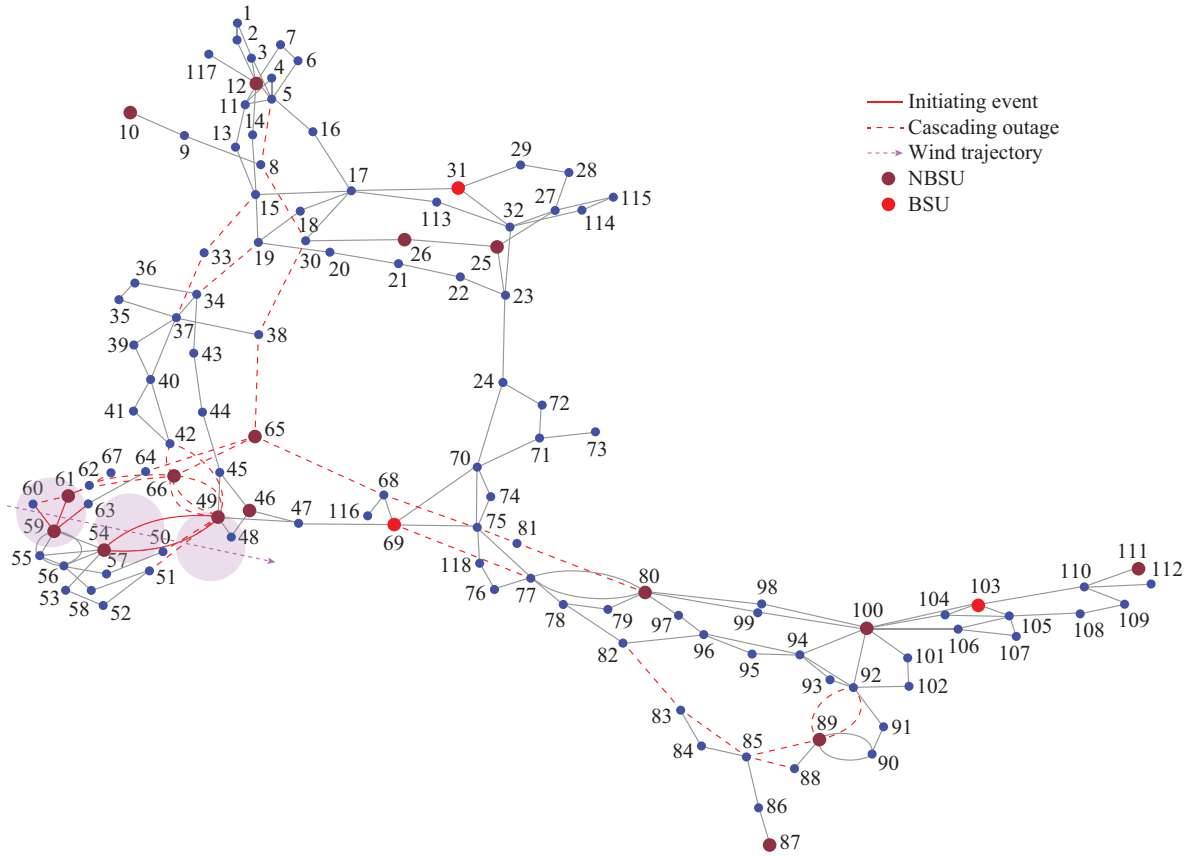


Fig. 14. Visualization of impacts of cascading failures on IEEE 118-bus system under initiating events without ICI.

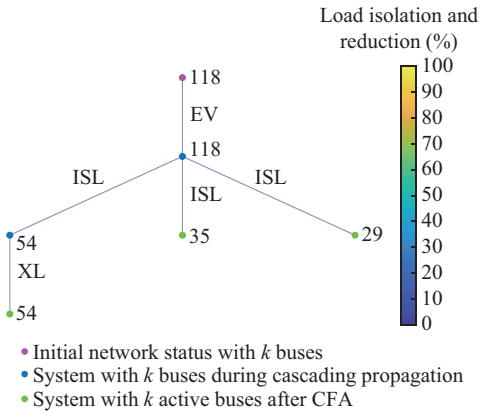


Fig. 15. Cascading failure analysis of IEEE 118-bus system under initiating events with ICI.

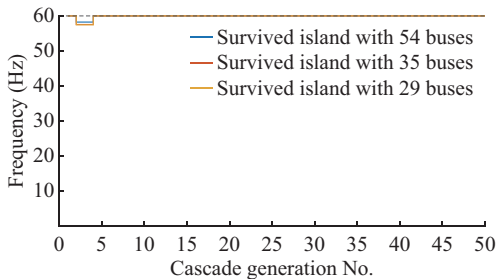


Fig. 16. System frequency for IEEE 118-bus system under initiating events with ICI.

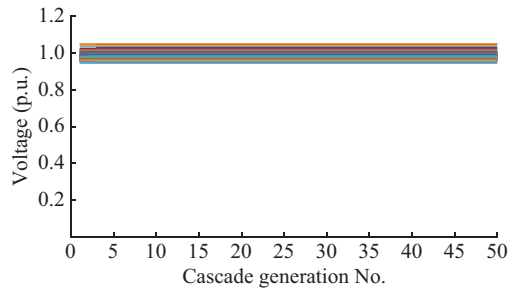


Fig. 17. Voltage profile of IEEE 118-bus system under initiating events with ICI.

Similarly, Fig. 24 compares the voltage profiles, showing stable post-islanding operation with the ICI. Notably, the proposed framework partially addresses uncertainty in initiating events through the weather-event simulator by varying storm parameters, but other uncertainties can also be incorporated. Probabilistic state estimation can account for measurement noise, scenario-based or stochastic optimization can support the decision-making and post-islanding optimization, and co-simulation with communication network models can evaluate the impact of latency on islanding actions.

IV. CONCLUSION

This paper proposes a holistic cascading-driven ICI framework for quantifying, detecting, and mitigating cascading impacts to enhance power grid resilience.

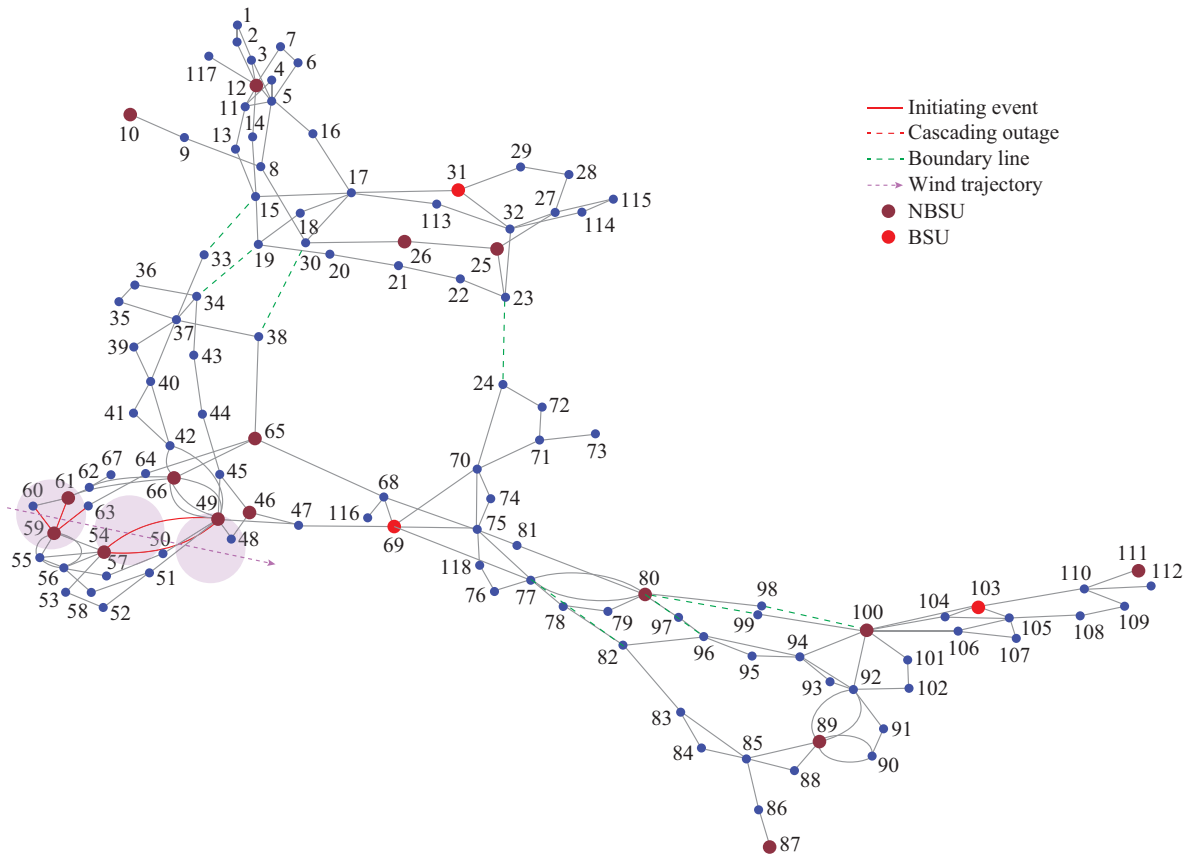


Fig. 18. Visualization of impacts of cascading failures on IEEE 118-bus system under initiating events with ICI.

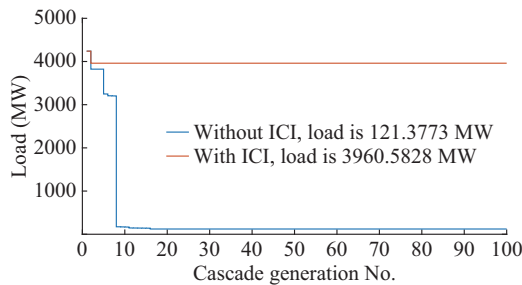


Fig. 19. Comparison of system resilience using trapezoid curve.

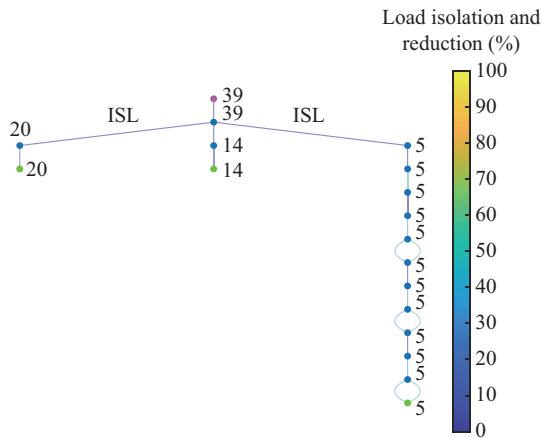


Fig. 20. Cascading failure analysis of IEEE 39-bus system under initiating events with SCICI.

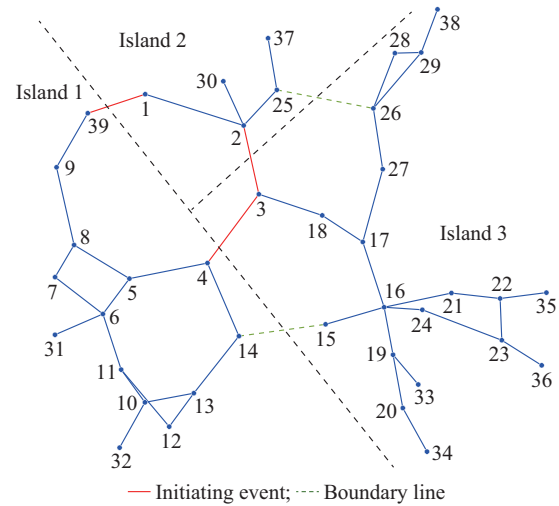


Fig. 21. Visualization of impacts of cascading failures on IEEE 39-bus system under initiating events with SCICI.

It leverages a novel ICI based on the decision-making mechanism that employs cascading failure metrics (size and grid integrity) to tailor effective MSs. If cascading failures can be halted solely through LR, then LR is recommended. Otherwise, if LR alone is insufficient and cascading outages spread, ICI (incorporating system splitting, LR, frequency reserve utilization, and generation rescheduling) is applied.

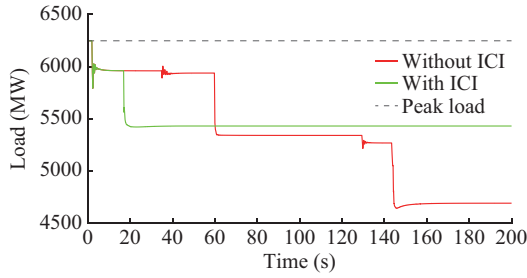


Fig. 22. System load of IEEE 39-bus system under initiating events with and without ICI.

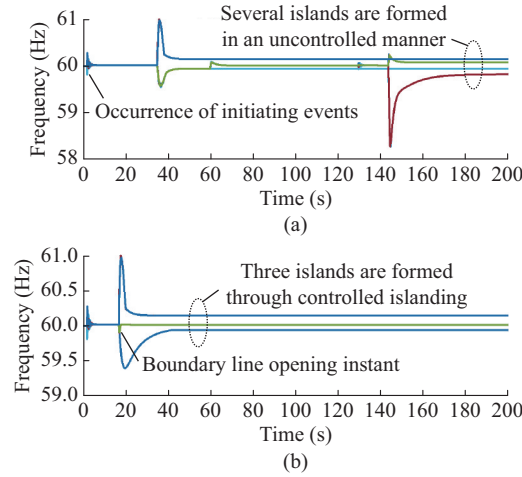


Fig. 23. Frequency responses of IEEE 39-bus system under initiating events with and without ICI. (a) Without ICI. (b) With ICI.

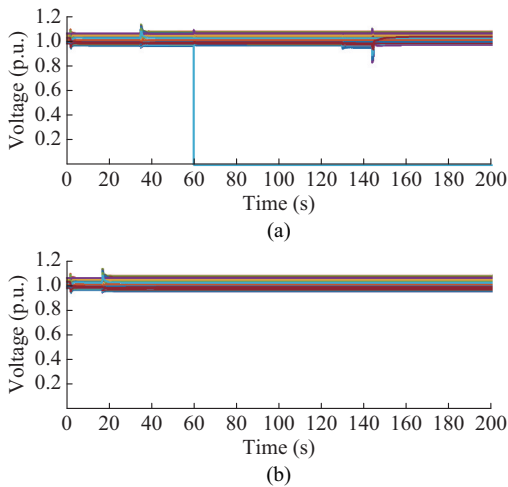


Fig. 24. Voltage profiles of IEEE 39-bus system under initiating events with and without ICI. (a) Without ICI. (b) With ICI.

The proposed framework can be applied in both short-term operational planning to assess the system under expected or anticipated events, as well as in near-real-time operations in the face of evolving events, with the aim of mitigating cascading blackouts. Its applicability is examined under a large set of contingencies including deterministic $N-k$ ($k \in [1, 3]$) and stochastic weather-related events (simulated up to $N-6$ contingencies). The results demonstrate how the framework can effectively enhance the reliability and resili-

ence of the test system by mitigating the impacts of expected events, thereby decreasing the mean value of DNS, as well as addressing unexpected tail-risk events. This involves curtailing the tail end of the probability density function curve of DNS and reducing the corresponding CVaR.

However, some aspects still remain unaddressed such as the risk of frequency-related cascading failures in low-inertia islands, particularly in power grids with high penetration of renewable energy sources, and data uncertainties (including missing or inaccurate data that may lead to state estimation errors and suboptimal decisions such as incorrect, delayed, or unnecessary decisions on system islanding). These aspects will be further explored in future work as extensions of this paper.

REFERENCES

- [1] H. Guo, C. Zheng, H. Iu *et al.*, "A critical review of cascading failure analysis and modeling of power system," *Renewable and Sustainable Energy Reviews*, vol. 80, pp. 9-22, Dec. 2017.
- [2] M. Panteli, D. N. Trakas, P. Mancarella *et al.*, "Boosting the power grid resilience to extreme weather events using defensive islanding," *IEEE Transactions on Smart Grid*, vol. 7, no. 6, pp. 2913-2922, Nov. 2016.
- [3] P. Dey, R. Mehra, F. Kazi *et al.*, "Impact of topology on the propagation of cascading failure in power grid," *IEEE Transactions on Smart Grid*, vol. 7, no. 4, pp. 1970-1978, Jul. 2016.
- [4] R. Yao, S. Huang, K. Sun *et al.*, "Risk assessment of multi-timescale cascading outages based on Markovian tree search," *IEEE Transactions on Power Systems*, vol. 32, no. 4, pp. 2887-2900, Jul. 2017.
- [5] J. Qi, W. Ju, and K. Sun, "Estimating the propagation of interdependent cascading outages with multi-type branching processes," *IEEE Transactions on Power Systems*, vol. 32, no. 2, pp. 1212-1223, Mar. 2017.
- [6] M. Noebels, R. Preece, and M. Panteli, "AC cascading failure model for resilience analysis in power networks," *IEEE Systems Journal*, vol. 16, no. 1, pp. 374-385, Mar. 2022.
- [7] J. Song, E. Cotilla-Sanchez, G. Ghanavati *et al.*, "Dynamic modeling of cascading failure in power systems," *IEEE Transactions on Power Systems*, vol. 31, no. 3, pp. 2085-2095, May 2016.
- [8] Y. Cai, Y. Li, Y. Cao *et al.*, "Modeling and impact analysis of interdependent characteristics on cascading failures in smart grids," *International Journal of Electrical Power & Energy Systems*, vol. 89, pp. 106-114, Jul. 2017.
- [9] A. Kyriacou, P. Demetriou, C. Panayiotou *et al.*, "Controlled islanding solution for large-scale power systems," *IEEE Transactions on Power Systems*, vol. 33, no. 2, pp. 1591-1602, Mar. 2018.
- [10] M. Sadeghi, H. Akbari, T. Daemi *et al.*, "An innovative mode-based coherency evaluation method for data-driven controlled islanding in power systems," *Electric Power Systems Research*, vol. 214, p. 108808, Jan. 2023.
- [11] M. R. Aghamohammadi, S. F. Mahdavi-zadeh, and Z. Rafiee, "Controlled islanding based on the coherency of generators and minimum electrical distance," *IEEE Access*, vol. 9, pp. 146830-146840, Oct. 2021.
- [12] Z. Wang and Z. Wang, "A novel preventive islanding scheme of power system under extreme typhoon events," *International Journal of Electrical Power & Energy Systems*, vol. 147, p. 108857, May 2023.
- [13] S. Admasie, S. B. Ali Bukhari, T. Gush *et al.*, "Intelligent islanding detection of multi-distributed generation using artificial neural network based on intrinsic mode function feature," *Journal of Modern Power Systems and Clean Energy*, vol. 8, no. 3, pp. 511-520, May 2020.
- [14] M. H. Oboudi, R. Hooshmand, and A. Karamad, "A feasible method for controlled intentional islanding in microgrids based on PSO algorithm," *Swarm and Evolutionary Computation*, vol. 35, pp. 14-25, Aug. 2017.
- [15] M. R. Aghamohammadi and A. Shahmohammadi, "Intentional islanding using a new algorithm based on ant search mechanism," *International Journal of Electrical Power & Energy Systems*, vol. 35, no. 1, pp. 138-147, Feb. 2012.
- [16] S. Ranjbar, "Online estimation of controlled islanding time intervals using dynamic state trajectories through cascading failures from

- WAMS data,” *Electric Power Systems Research*, vol. 214, p. 108890, Jan. 2023.
- [17] X. Han, Q. Huang, X. Duan *et al.*, “Intentional controlled islanding based on dynamic community detection for power grid,” *IET Generation, Transmission & Distribution*, vol. 16, no. 21, pp. 4258-4272, Nov. 2022.
- [18] S. Kamali, T. Amraee, and M. Fotuhi-Firuzabad, “Controlled islanding for enhancing grid resilience against power system blackout,” *IEEE Transactions on Power Delivery*, vol. 36, no. 4, pp. 2386-2396, Aug. 2021.
- [19] F. Teymouri, T. Amraee, H. Saberi *et al.*, “Toward controlled islanding for enhancing power grid resilience considering frequency stability constraints,” *IEEE Transactions on Smart Grid*, vol. 10, no. 2, pp. 1735-1746, Mar. 2019.
- [20] H. Golpîra, “A data-driven based approach for islanding detection in large-scale power systems,” *IEEE Transactions on Power Systems*, vol. 40, no. 1, pp. 272-285, Jan. 2025.
- [21] L. Niu, D. Sahanbandu, A. Clark *et al.*, “A hybrid submodular optimization approach to controlled islanding with post-disturbance stability guarantees,” *IEEE Transactions on Power Systems*, vol. 39, no. 2, pp. 4486-4497, Mar. 2024.
- [22] S. Xu and S. Miao, “Three-stage method for intentional controlled islanding of power systems,” *Journal of Modern Power Systems and Clean Energy*, vol. 6, no. 4, pp. 691-700, Jul. 2018.
- [23] M. Yoon, X. Zhang, and S. Choi, “Strategic intentional islanding method considering temporary overvoltage in disaster situations,” *International Journal of Electrical Power & Energy Systems*, vol. 165, p. 110488, Apr. 2025.
- [24] H. Hua, Y. Qin, Z. He *et al.*, “Energy sharing and frequency regulation in energy network via mixed H_2/H_∞ control with Markovian jump,” *CSEE Journal of Power and Energy Systems*, vol. 7, no. 6, pp. 1302-1311, Nov. 2021.
- [25] ENTSO-E. (2010, Aug.). Operation handbook: policy 5 – emergency operations, final version. [Online]. Available: https://eepublicdownloads.entsoe.eu/clean-documents/pre2015/publications/entsoe/Operation_Handbook/Policy_5_final.pdf
- [26] ENTSO-E. (2006, May). Policy 5: emergency operations, ENTSO-E operational handbook. [Online]. Available: https://eepublicdownloads.entsoe.eu/clean-documents/pre2015/publications/ce/oh/Policy5_v1.0_03.05.2006.pdf
- [27] *IEEE Standard for Interconnection and Interoperability of Distributed Energy Resources with Associated Electric Power Systems Interfaces*, IEEE Std. 1547-2018, 2018.
- [28] NERC. (2017, Apr.). EOP-011-1: emergency operations. [Online]. Available: https://www.nerc.com/pa/stand/reliability_standards/eop-011-1.pdf
- [29] NERC. (2017, Apr.). EOP-011-2: emergency operations. [Online]. Available: https://www.nerc.com/pa/stand/reliability_standards/eop-011-2.pdf
- [30] ISO-NE. (2025, Jun.). OP-19: operating procedures. [Online]. Available: https://www.iso-ne.com/rules_proceeds/operating/isone/op19/op19_rto_final.pdf
- [31] M. Panteli and P. Mancarella, “Modeling and evaluating the resilience of critical electrical power infrastructure to extreme weather events,” *IEEE Systems Journal*, vol. 11, no. 3, pp. 1733-1742, Sept. 2017.
- [32] E. W. Dijkstra, “A note on two problems in connexion with graphs,” *Numerische Mathematik*, vol. 271, pp. 269-271, Dec. 1959.
- [33] M. Panteli, C. Pickering, S. Wilkinson *et al.*, “Power system resilience to extreme weather: fragility modeling, probabilistic impact assessment, and adaptation measures,” *IEEE Transactions on Power Systems*, vol. 32, no. 5, pp. 3747-3757, Sept. 2017.
- [34] K. Knapp, M. Kruk, D. Levinson *et al.*, “The international best track archive for climate stewardship (IBTrACS): unifying tropical cyclone data,” *Bulletin of the American Meteorological Society*, vol. 91, pp. 363-376, Mar. 2019.
- [35] M. C. K. J. Gahtan, K. R. Knapp, C. J. Schreck *et al.* (2024, Dec.). International best track archive for climate stewardship (IBTrACS). [Online]. Available: <https://www.ncei.noaa.gov/products/international-best-track-archive>
- [36] X. Mao, W. Zhu, L. Wu *et al.*, “Comparative study on methods for computing electrical distance,” *International Journal of Electrical Power & Energy Systems*, vol. 130, p. 106923, Sept. 2021.
- [37] H. S. Park and C. H. Jun, “A simple and fast algorithm for K-medoids clustering,” *Expert Systems with Applications*, vol. 36, no. 2, pp. 3336-3341, Mar. 2009.
- [38] J. Hedengren. (2024, Dec.). MINLP: mixed integer nonlinear programming. [Online]. Available: <https://www.mathworks.com/matlabcentral/fileexchange/35720-minlp-mixed-integer-nonlinear-programming>
- [39] R. D. Zimmerman, C. E. Murillo-Sánchez, and R. J. Thomas, “MATPOWER: steady-state operations, planning, and analysis tools for power systems research and education,” *IEEE Transactions on Power Systems*, vol. 26, no. 1, pp. 12-19, Feb. 2011.
- [40] D. Chen and K. Ding, *System Stability and Control Technologies After Large-scale Wind Power Integration*. Beijing: China Electric Power Press, 2015.
- [41] M. Noebels, I. Dobson, and M. Panteli, “Observed acceleration of cascading outages,” *IEEE Transactions on Power Systems*, vol. 36, no. 4, pp. 3821-3824, Jul. 2021.
- [42] Y. Xie, D. Li, Y. Xu *et al.*, “A MILP-based restoration planning method for generator start-up considering flexible re-energizing times of transmission lines,” *International Journal of Electrical Power & Energy Systems*, vol. 124, p. 106357, Jan. 2021.
- [43] R. Moreno, M. Panteli, P. Mancarella *et al.*, “From reliability to resilience: planning the grid against the extremes,” *IEEE Power and Energy Magazine*, vol. 18, no. 4, pp. 41-53, Jul. 2020.
- [44] A. Esmacilian and M. Kezunovic, “Prevention of power grid blackouts using intentional islanding scheme,” *IEEE Transactions on Industry Applications*, vol. 53, no. 1, pp. 622-629, Jan.-Feb. 2017.

Sina Hashemi received the Ph.D. degree in power system stability and control from the University of Tehran, Tehran, Iran, in 2022. He is currently a Senior Research Associate at the KIOS Research and Innovation Center of Excellence, University of Cyprus, Nicosia, Cyprus. His research interests include power grid resilience assessment and enhancement, with expertise in cascading failure modeling and analysis, cyber-attack-induced cascading failure mitigation, and cost-benefit analysis of hybrid AC/DC power grid.

Balaji V. Venkatasubramanian is currently a Research Associate with the KIOS Research and Innovation Center of Excellence, University of Cyprus, Nicosia, Cyprus. His main research interests include power system resilience, grid operability and compliance, renewable integration, and energy storage planning.

Pierluigi Mancarella received the M.Sc. and Ph.D. degrees in electrical energy systems from Politecnico di Torino, Torino, Italy, and was a Post-doc Research Associate at Imperial College London, London, U.K.. He is currently Chair Professor of Electrical Power Systems at The University of Melbourne, Melbourne, Australia, and Professor of Smart Energy Systems at The University of Manchester, Manchester, U.K.. His research interests include multi-energy system, grid integration of renewable energy, energy infrastructure planning under uncertainty, and reliability and resilience assessment of low-carbon network.

Mathaios Panteli is currently an Assistant Professor with the Department of Electrical and Computer Engineering, University of Cyprus, Nicosia, Cyprus, and a Faculty Member of the KIOS Research and Innovation Center of Excellence, University of Cyprus. His main research interests include techno-economic reliability, resilience and flexibility assessment of future low-carbon energy system, grid integration of renewable energy, and integrated modelling and analysis of co-dependent critical infrastructures.